Desalination and Water Treatment
www.deswater.com
doi: 10.5004/dwt.2019.23849

157 (2019) 219–227
July

Research on the expansion mechanism of hydraulic fracture branching induced by weak bedding shear slip

Suling Wang[a], Jinbo Li[a], Kangxing Dong[a,*], Qinghai Yang[b]

[a]*Institute of Mechanical Science and Engineering, Northeast Petroleum University, Daqing 163318, China, email: dongkangxing@163.com (K. Dong)*
[b]*CNPC Petroleum Exploration and Production Research Institute, Beijing 100083, China*

Received 22 October 2018; Accepted 15 January 2019

ABSTRACT

Bedding fracture is the main rock mass of the tight reservoir; the main method for the formation of complex fractures of dense rock is to activate weak bedding to induce the branch extension of hydraulic fracture. Based on fracture mechanics, this paper established the mechanical model of coupled extension with weak bedding when the hydraulic fracture is close to the weak bedding process, adopted the numerical analysis method, based on the equivalent principle of coupling, through unit compilation techniques, and realized the numerical simulation of the expansion of hydraulic fracture and weak bedding. The results show that the hydraulic fracture tip passivation is induced by shear slip of weak bedding plane; the increase of shear stress in the weak bedding is the main control mechanism of the expansion of hydraulic fracture; the closer the approaching angle, the greater the elastic modulus of reservoir, and the lower the stress difference, the more difficult it is to induce weak bedding shear damage. The greater the viscosity of the fracturing fluid, the greater the displacement, the more prone to inducing shear damage of weak bedding plane, and the more complex the formation of cracks.

Keywords: Dense reservoir; Weak bedding; Shear fracture; Fracture network; Numerical simulation

1. Introduction

In the conventional reservoir hydraulic fracture theory, the open fracture mechanism of hydraulic fractures is mainly studied but less research on shear failure [1–3]. Non-conventional shale or tight rock reservoirs contain structural weak surfaces such as natural fractures or bedding. During the fracturing process, shear failure is easy to occur, and hydraulic cracks are communicated with each other to form network cracks. Murphy et al. believe that rock rupture is the result of shearing, especially in fractured reservoirs, where fracturing is the shear slip of rock along the joint plane [4]. Warpinski also verified through laboratory experiments that there are three extension modes for hydraulic cracks under the influence of natural cracks: through natural cracks, opened natural cracks prevent expansion, natural cracks that are damaged by shear prevent expansion [5]. Dyneshy believes that the mechanism of unsteady expansion of hydraulic fractures is shear failure of rocks [6,7]. Warpinski believes that natural cracks are prone to shear failure when hydraulic cracks interfere with natural cracks, and the influence of fluid loss on stress fields is also discussed [5]. Zhou, Chen, and others analyzed the mechanism of shear fracture caused by hydraulic cracks through theoretical and experimental methods and discussed its influencing factors [8]. Wei Rui analyzed the influence of natural cracks or joint shear slip on the conductivity of fractures [9]. Anderson, Renshaw, Peng, Cheng, and other domestic and foreign scholars also theoretically analyzed the occurrence conditions of natural fracture shear failure [10–22].

* Corresponding author.

In summary, domestic and foreign scholars have given the extended behavior of hydraulic fractures after encountering natural cracks through theoretical analysis and experimental research, and given the criteria for shear failure of natural fractures, however, there are few studies on the mechanism of coupling and expansion of natural cracks and hydraulic cracks. In this paper, the fluid-solid coupling effect of hydraulic fracturing and the interaction between hydraulic fracture and weak bedding are considered. Establishing a calculation model for the expansion of hydraulic fracture and weak layer intersection, the variation process of stress and displacement of weak layer in hydraulic fracturing process is analyzed. The coupling mechanism between weak bedding and hydraulic fracture is analyzed, which provides theoretical support for the formation of complex fractures in unconventional reservoir hydraulic fracturing.

2. Establishment of coupled mechanical model for hydraulic fracture and weak bedding

In the tight reservoirs, the development of layered cracks is dominant and the structural joints and natural fractures are weakly developed. In the hydraulic fracturing of tight reservoirs, under the action of hydraulic cracks, the weak bedding is activated, and the weak mechanical behavior of the weak layer determines the extended form of the hydraulic fracture through weak bedding; this is a mechanical problem of hydraulic fracture and weak bedding coupling.

The space diagram of hydraulic crack and weak layer intersection is shown in Fig. 1, taking the type of horizontal fault normal stress in horizontal well as an example ($\sigma_v > \sigma_Y > \sigma_X$) and taking the three principal stress directions of the space as the coordinate axis directions ($\sigma_Z = \sigma_3$, $\sigma_Y = \sigma_2$, $\sigma_X = \sigma_1$). The wellbore direction is along with the direction of minimum principal stress, the hydraulic fracture extends in the *YZ* plane perpendicular to the minimum principal stress, the angle between natural cracks and hydraulic cracks is α, taking a symmetry plane perpendicular to the plane of the crack and the weak plane, the hydraulic crack propagation on this plane satisfies the plane strain, establish an extended mechanical model of the intersection of hydraulic fracture and weak layer, as shown in Fig. 2.

Before the hydraulic crack and the weak layer meet, the hydraulic crack is a type I tensile failure crack. According to the linear elastic fracture mechanics, in the polar coordinate system, the stress field of the type I crack tip is

$$\begin{cases} \sigma_{n\text{tip}} = \dfrac{K_1}{\sqrt{2\pi r}}\cos^3\dfrac{\theta}{2} \\ \tau_{\text{tip}} = \dfrac{K_1}{2\sqrt{2\pi r}}\cos\dfrac{\theta}{2}\sin\theta \end{cases} \tag{1}$$

The weak layer is a discontinuous plane in the rock mass structure. During the process of hydraulic crack approaching the weak layer, the stress generated on the weak layer mainly includes three parts: (1) Pre-stress in the weak bedding plane under the action of far field stress; (2) Stress induced by the stress field at the tip of the hydraulic fracture; (3) The osmotic pressure generated by the fracturing fluid pressure. According to the linear elastic fracture mechanics, the stress acting on the weak bedding plane is

$$\begin{cases} \sigma_n = \dfrac{\sigma_1+\sigma_3}{2} - \dfrac{\sigma_1-\sigma_3}{2}\cos 2\alpha + \dfrac{K_1}{\sqrt{2\pi r}}\cos^3\dfrac{\theta}{2} - p(r) \\ \tau^{\mp} = -\dfrac{\sigma_1-\sigma_3}{2}\sin 2\alpha \pm \dfrac{K_1}{2\sqrt{2\pi r}}\sin\dfrac{\theta}{2}\sin\theta \end{cases} \tag{2}$$

where "–" represents the left weak layer; "+" represents the right weak layer; σ_n normal stress on weak bedding plane under far field stress, MPa; $\tau^{\mp}$ shear stress of weak bedding plane under far field stress, MPa; σ_1 is the maximum principal stress of the reservoir, MPa; σ_3 is the minimum principal stress of the reservoir, MPa; α is the angle between the weak bedding and the minimum principal stress of the reservoir, degree.

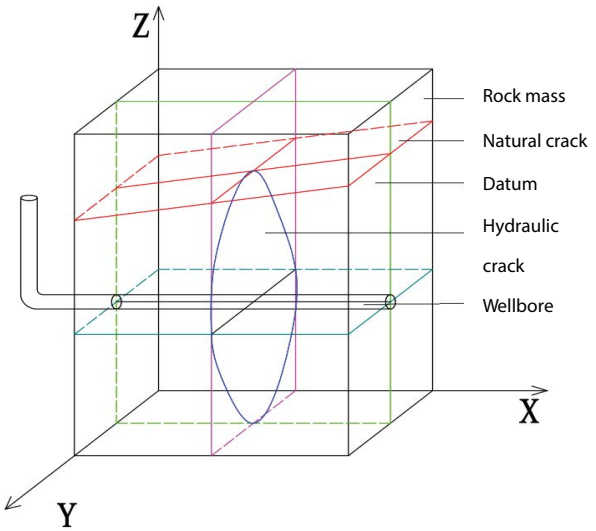

Fig. 1. The space diagram of hydraulic crack and weak layer intersection.

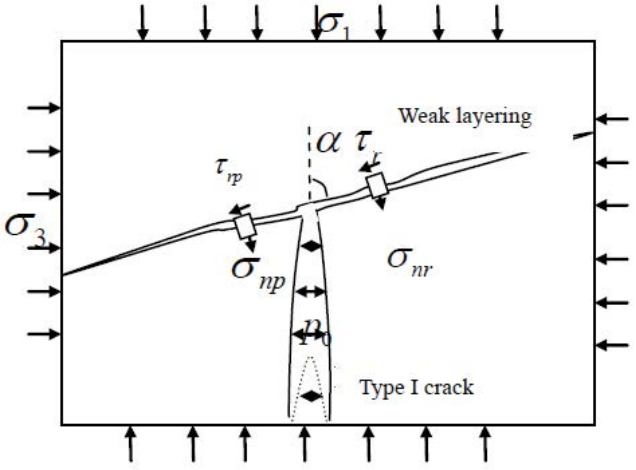

Fig. 2. Extended mechanical model of hydraulic fracture and weak layer intersection.

Hydraulic shear cracking slip on the weak bedding plane needs to meet two conditions: (1) the maximum principal stress at the tip of the hydraulic fracture is less than the tensile strength of the formation and (2) the shear stress generated by the weak bedding plane is greater than the shear strength of the interface, therefore,

$$\sigma_s\big|_{\theta=0} < T \tag{3a}$$

$$\tau^{\pm} \geq \tau_0 + K_f \sigma_n \tag{3b}$$

Here σ_S is the maximum principal stress at the tip of the crack, MPa; T is rock tensile strength, MPa; τ_0 is the shear strength of the weak interface, Mpa; and K_f the friction coefficient of the interface is dimensionless.

The distribution of normal stress and shear stress distribution on the bedding plane can be determined by Eq. (2). When the shear stress and the normal stress satisfy Eqs. 3(a) and (b), the shear failure occurs in the weak bedding and the hydraulic crack will extend along the weak bedding plane. Otherwise, no shear damage occurs in the weak bedding plane, and hydraulic cracks extend through the weak layer.

3. Numerical calculation of hydraulic fracture and weak layer intersection

The weak layer structure makes the matrix of the rock mass heterogeneous. Therefore, based on the above theoretical analysis and numerical analysis technology, a numerical calculation model for the intersection of hydraulic fracture and natural fracture is established to analyze the coupling between hydraulic fracture, weak bedding, and the extended behavior; numerical model is shown in Fig. 3. The difficult point in the calculation of fracture mechanics is the intersection of cracks. In this paper, the cohesion unit is used to simulate hydraulic cracks and weak bedding. The cohesive element can represent the irregularly distributed weak bedding as a continuous function of the normal section line, weights the internal friction angle and cohesion force of the weak bedding into the anisotropic strength parameters of the material, and recompiles the unit at the junction by the unit compiling technique to make the fluid at the junction according to the damage condition of the cohesive unit, the flow direction is selected. The flow is reasonably distributed to realize the branching and intersection of the crack.

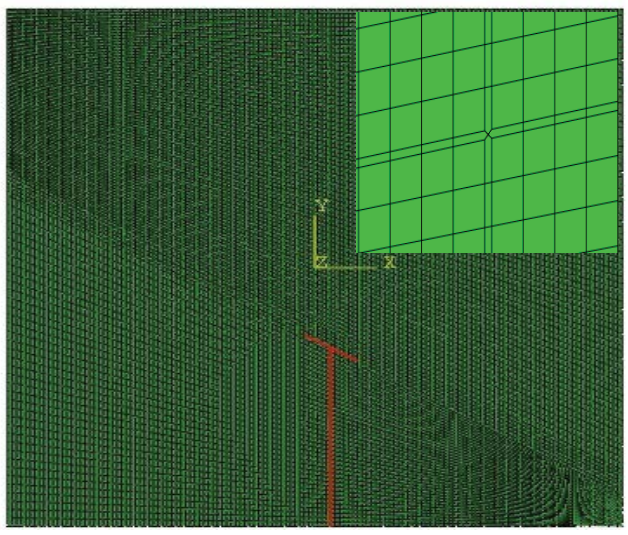

Fig. 3. Numerical model for the extension of hydraulic fracture and weak layer intersection.

The propagation model of fracturing fluid in a cross-fracture is shown in Fig. 4. According to Kirchhoff's first and second laws, the total flow rate injected is equal to the sum of the flow rates of each branch fracture.

$$q_0 = q_1 + q_2 + q_3 \tag{4}$$

In the formula, q_0 is the main fracture flowing, m^3/s; q_1, q_2, q_3 are the flow of branch cracks, m^3/s.

The flow of each branch crack follows the Newtonian flow formula:

$$q_n = \frac{d_n^2}{12\mu} \nabla p_n \tag{5}$$

Here q_n is the branch crack flow, m^3/s; d_n is the opening degree of the branch crack, m; ∇p_n is the fluid pressure gradient of the branch crack, Pa.

The calculation process is divided into two steps: the first step is to apply the gravity field and the initial geostress field to simulate the existing stress field in the formation and the second step is to use the transient analysis method to inject the fracturing fluid to simulate the fracturing process. With the injection of fracturing fluid, the cohesive force gradually damages and the stiffness decreases. When the damage value reaches 1, the material breaks, macroscopic cracks appear, and the fracturing fluid flows into the crack.

4. The analysis of hydraulic crack and bedding cross-expansion results

The strength of the bedding plane is the main controlling factor for the change of hydraulic crack propagation.

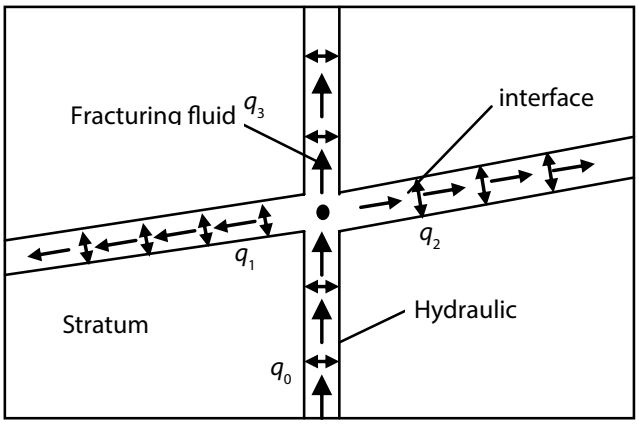

Fig. 4. Flowing of fracturing fluid in cracks.

According to the digital speckle test, the ratio of the tensile strength of the layer to the tensile strength of the rock mass is taken as the quantitative value of the interface strength, and the strength is reduced. The coefficients were 0.3 and 0.8 selected for calculation. The calculation parameters are shown in Table 1.

4.1. Analysis of interface stress state under initial ground stress

According to the established hydraulic fracture and weak bedding convergence model and according to the parameters of Table 1, when the strength reduction coefficient is 0.3, after the ground stress balance, under the action of the far site stress, the normal stress on the bedding plane is 19.86 MPa, shear stress is 0.5 MPa, and the shear stress distribution of the weak bedding plane is shown in Fig. 5. According to the elastic two-dimensional linear elastic model, the theoretically calculated normal stress is 18.92 MPa, the shear stress is 0.49 MPa, and the errors are 5% and 2%. The rationality of the model was verified.

4.2. Intersecting and expanding analysis of hydraulic cracks and bedding surfaces

According to the analysis of the foregoing theory, the normal stress and shear stress on the bedding surface are changed under the induction of hydraulic cracks; the local position of the hydraulic cracks and natural cracks is analyzed. Fig. 6 shows the change of pore pressure at different times of the interface layer when alpha = 0.3, and Fig. 7 shows the interface damage at different times of the interface layer when alpha = 0.3.

As can be seen from Figs. 6 and 7, the hydraulic fracture intersects with the weak bedding in 19.64 s, the fracturing fluid acts in the matrix crack, and the weak bedding does not enter the fluid and does not damage. At the time of 23.64 s, the pore pressure in the right weak bedding surface increases and the fracturing fluid enters the weak bedding on the right side, causing the weak bedding surface to destroy on the right

Table 1
Intersection of fractures to expand reservoirs and bedding parameters

Reservoir elastic modulus/E 40 GP
Poisson's ratio/μ 0.21
Saturation factor/B 1.0
Reservoir permeability coefficient/K 1.0
Reservoir porosity/Φ 0.1
Reservoir fluid compressibility incompressible
Reservoir tensile strength/σ_{tcc} 3.5 MPa
Maximum horizontal stress/σ_H 20 MPa
Minimum horizontal stress/σ_h 18 MPa
Bedding strength reduction factor/α 0.3/0.8
Bedding angle/θ 75°
Fracturing fluid displacement/q 2.4
Fracturing fluid viscosity/μ_{ky} l 20 MPa•s
Fracturing fluid loss factor/C_l 5.879e^{-10}

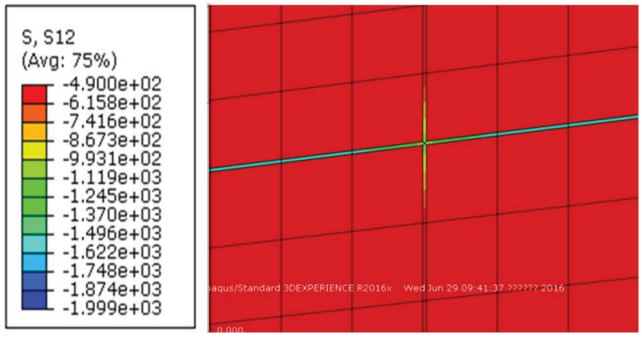

Fig. 5. Weak shear stress after balance of ground stress.

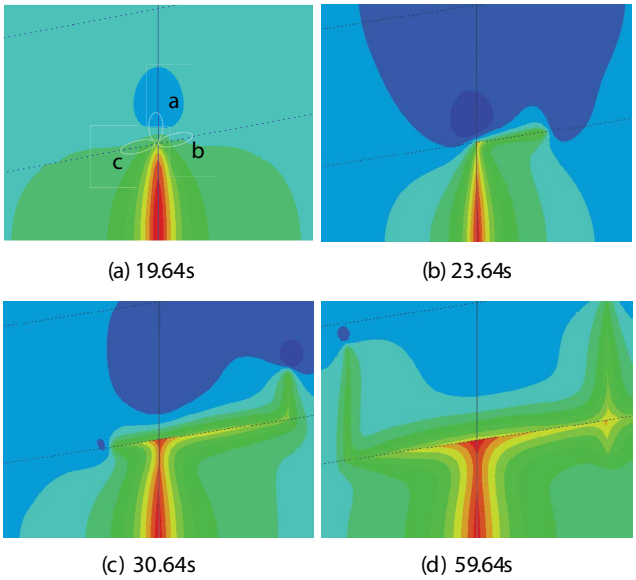

Fig. 6. Pore pressure distribution at different time in alpha = 0.3.

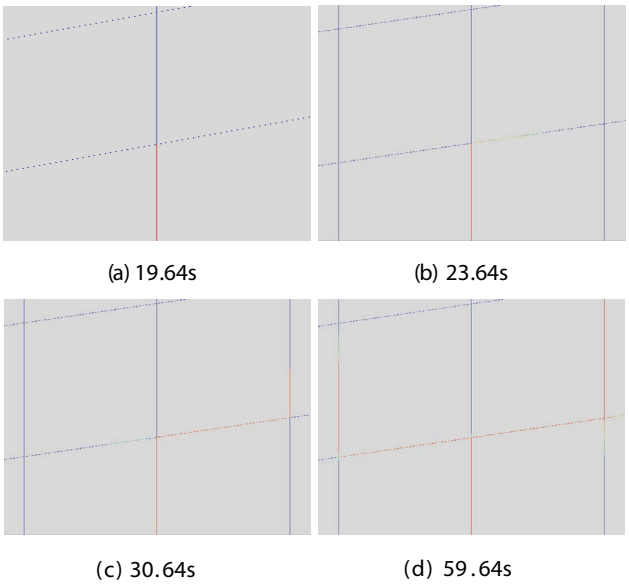

Fig. 7. Stiffness distribution of cohesive element at different moments at alpha = 0.3.

side; at 30.64 s, when the hydraulic crack extends a certain distance along the weak bedding surface, it breaks again to the maximum principal stress direction. At 59.64 s, the pore pressure of the weak bedding is increased, the interface is damaged, and the hydraulic crack is branched and expanded at the weak bedding.

The stress changes at the intersection of hydraulic fracture and weak bedding *a* (front end), *b* (left wing), and *c* (right wing) are extracted. As shown in Fig. 8, the crack tip opening displacement after hydraulic fracture and weak bedding intersection is shown in Fig. 8.

It can be seen from Fig. 8 that (1) during the coupling of hydraulic crack and weak bedding, the compressive stress at the tip of the crack gradually decreases. (2) The compressive stress of the right and left cracks of the hydraulic crack

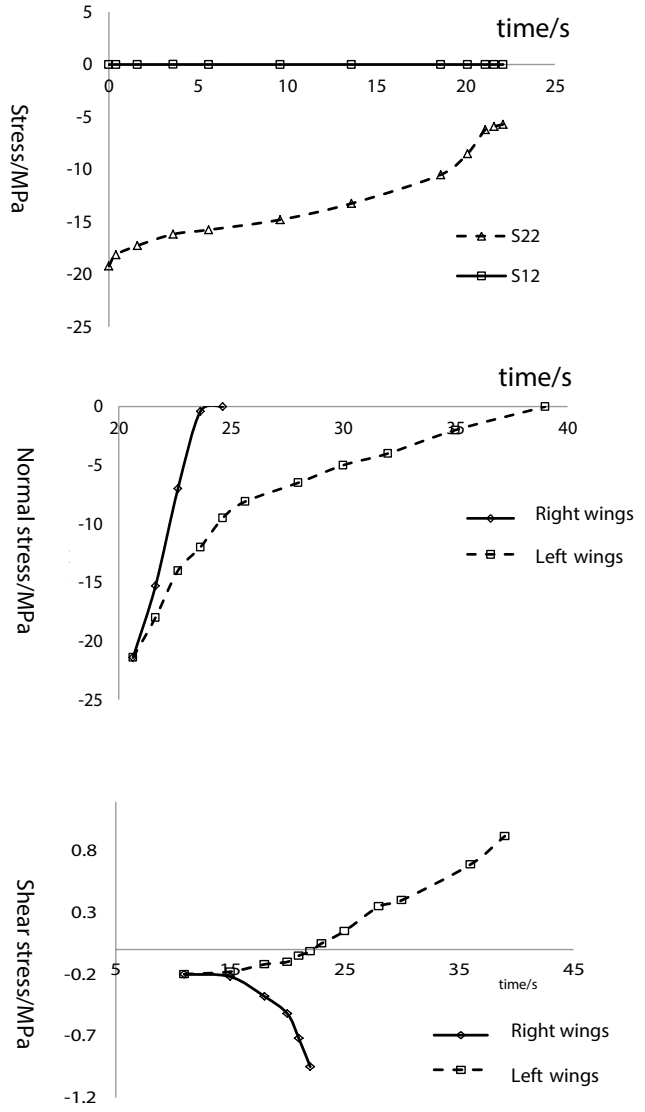

Fig. 8. Stress comparison of weak interfacial layer under hydraulic crack(a) Strain change at the front end of crack at α = 0. 3, (b) Normal stress comparison between left and right wings with α = 0. 3 and (c) Comparison of shear stress between left and right wings at α = 0. 3.

increases gradually due to the weak bedding. There is an angle with the hydraulic crack, which makes the left-wing weak layer and the right-wing weak layer asymmetry, and the compressive stress of the right-wing weak layer is reduced faster. (3) The hydraulic fracture tip was blunted at the weak bedding position because the weak of the bedding strength. The opening displacement is shown in Fig. 9. The opening width of the crack increases, so that the right-wing weak bedding is opposite to the shear slip direction of the left-wing weak bedding, resulting in the right-wing weak bedding. The shear stress increases, and the shear stress of the weak bedding on the left side decreases. After the weak bedding plane is activated, the open displacement increases gradually.

According to Eq. (3) and Fig. 8, before the weak bedding plane is activated, the bedding plane is in a compressive stress state, which is smaller than the rock tensile strength; the hydraulic fracture cannot extend through the weak bedding plane and the compressive stress of the surface is reduced rapidly and the shear stress is increased of the right-wing weak layer. The compressive stress of the surface is reduced rapidly and the shear stress is increased. According to the Mohr-Coulomb Theorem, the normal stress is reduced, the shear strength is also reduced, and the threshold of shear failure is weakened, while the normal stress of right wing reduced faster, so the right-wing weak bedding plane undergoes shear failure before the left wing. It can be seen that for the hydraulic crack and the weak bedding plane intersect, the weak hydraulic crack first spreads on one side of the weak bedding plane.

Enhancing interface strength, when the interface strength reduction coefficient is 0.8, the cross-expansion pattern of hydraulic crack and bedding plane is calculated. Fig. 10 shows the pore pressure distribution at different time points of the layered surface when α = 0.8.

It can be seen from Fig. 10 that when the strength of the bedding plane is high, the stress transmission capability is strong and the phenomenon of expansion cracking of the hydraulic crack at the interface is not obvious. The crack opening width is shown in Fig. 11, compared with the weak bedding plane, at 23.64 s. The hydraulic crack width of the weak layer is 0.0085 m, the hydraulic crack width of the strong bedding plane is 0.00085 m, and the phase difference is 10 times. Therefore, the stress concentration effect at the hydraulic crack tip is strong.

Figs. 12 and 13 show the state of stress change at the position of the hydraulic crack tip and the right-wing plane.

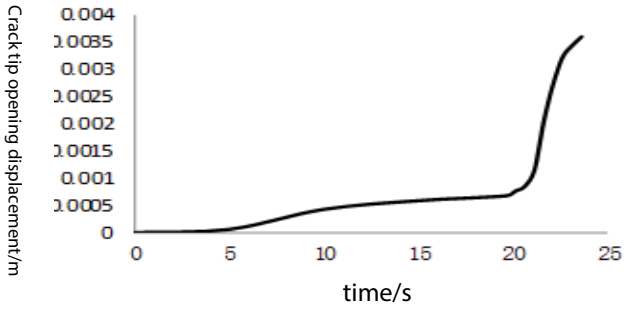

Fig. 9. Trend of crack tip opening displacement when α = 0.3.

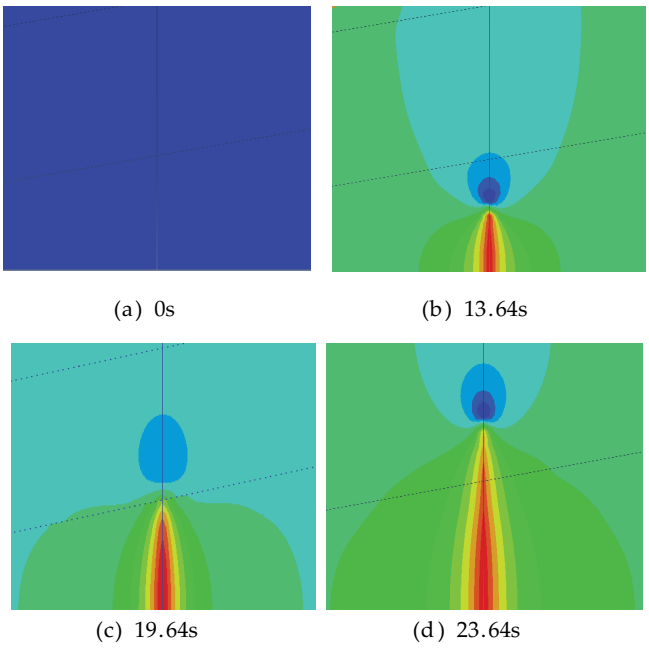

Fig. 10. Pore pressure distribution at different time points of the layered surface at $\alpha = 0.8$.

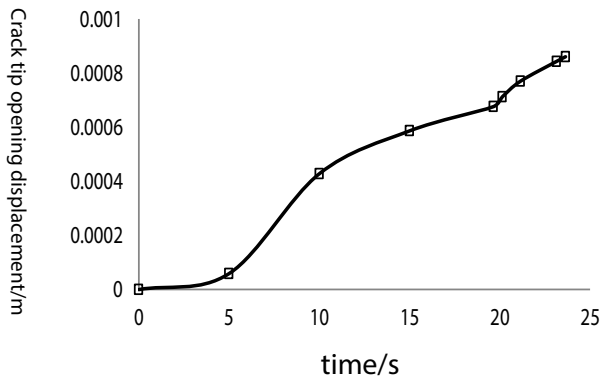

Fig. 11. Crack tip opening displacement when $\alpha = 0.8$.

It can be seen from Figs. 12 and 13 that the normal stress at the tip of the hydraulic crack changes from the compressive stress state to the tensile stress state, reaching the rock's tensile strength of the body; while the normal stress of the hydraulic layer on the right-wing layer increases, the compressive stress state gradually weakens, reducing the shear strength of the crack, but the shear stress increases less, and it is not easy to cause interface shear damage, according to Eq. (3). It can be seen that the hydraulic crack propagates through the bedding plane.

5. Analysis of factors affecting crack turn

Activating weak bedding is the key to improve the complexity of hydraulic fractures, according to the foregoing theoretical analysis. Under a certain interface strength, the approach angle, horizontal principal stress difference, net

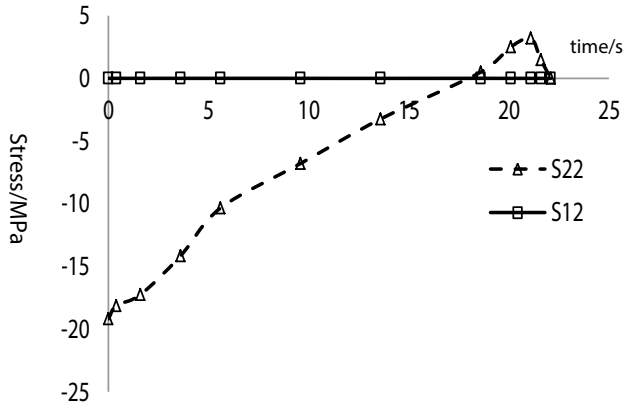

Fig. 12. Stress change of the front end of the hydraulic crack at $\alpha = 0.8$.

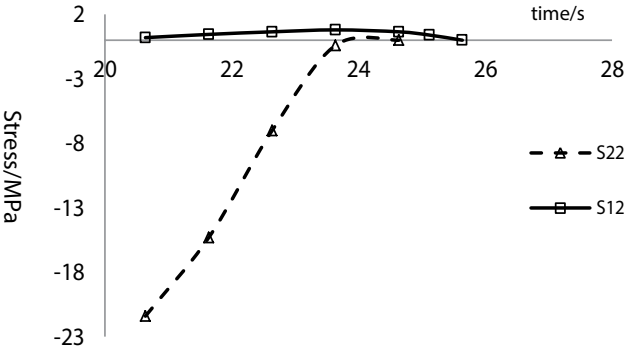

Fig. 13. Stress change of right-wing strong bedding unit with $\alpha = 0.8$.

pressure, and rock mechanic parameters of hydraulic cracks and weak bedding planes all affect the stress state after the intersection of hydraulic cracks and bedding planes. The following calculation is performed with a bedding plane strength reduction factor of 0.3.

5.1. Effect of elastic modulus on interface shear failure

According to the above parameters, select the approximation angles, which are 30°, 45°, 60°, and 75°, and the elastic moduli, which are 30 GPa, 40 GPa, 50 GPa, and 60 GPa, to begin the calculation. Under different approximation angles, the crack propagation width after the intersection of hydraulic cracks and bedding is shown in Fig. 14.

It can be seen from the single curves in Figs. 14 and 15 that as the hydraulic crack and the weak bedding approach angle increase, the hydraulic crack width gradually decreases. When the hydraulic crack and the weak interfacial layer meet, the passivation phenomenon is weaker. The minimum horizontal principal stress difference required for shear failure in weak bedding is gradually reduced, and the weaker bedding is less prone to shear failure. Therefore, the larger the approach angle, the less likely the shear failure occurs; the larger the reservoir elastic modulus, the smaller the hydraulic crack width, and the easier it is to form long and

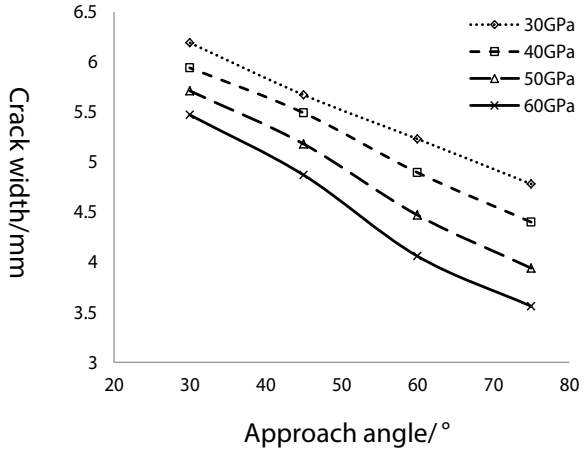

Fig. 14. Hydraulic crack width under different elastic modulus.

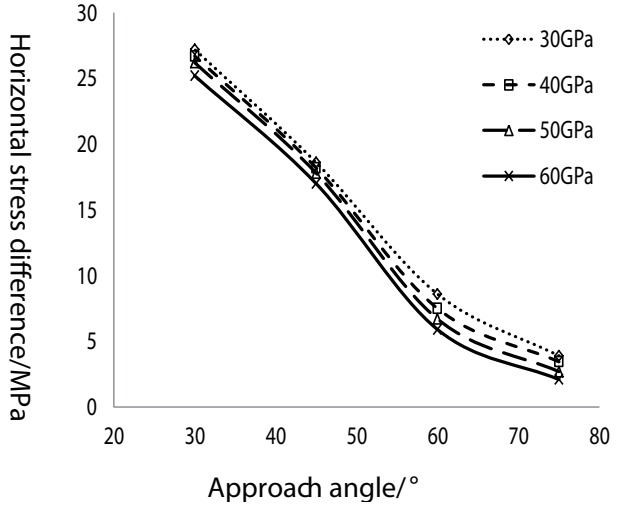

Fig. 15. Weak bedding shear failure conditions under different elastic modulus.

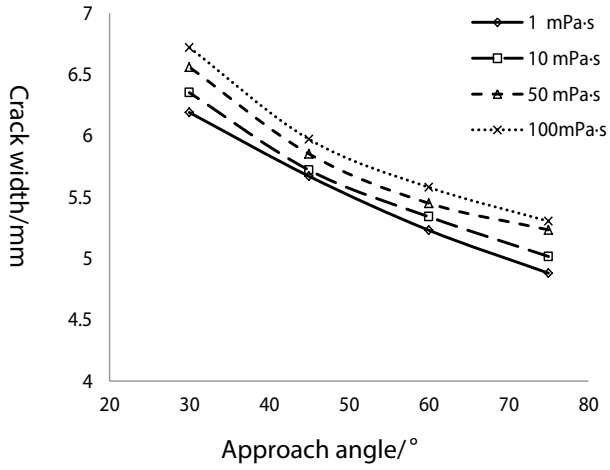

Fig. 16. Hydraulic crack width under different fracturing fluid viscosity.

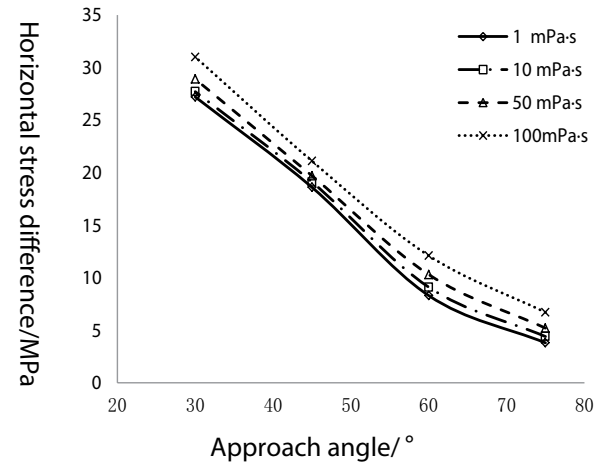

Fig. 17. Weak bedding shear failure conditions under different fracturing fluid viscosity.

narrow cracks. When the hydraulic crack and the weak layer meet, the passivation phenomenon is weaker, and the smaller the minimum principal stress difference of the shear failure, the weaker the layer is less prone to shear failure.

5.2. Influence of viscosity of fracturing fluid on interfacial shear failure

The frictional resistance of different fracturing fluids flowing in cracks is also different, resulting in different fluid pressure gradients in the cracks, which will have a certain impact on the crack propagation pattern. Different fracturing fluid viscosity and analysis of its influence on shear failure were selected. Calculated results are shown in Figs. 16 and 17.

It can be seen from Figs. 16 and 17 that the viscosity of the fracturing fluid is 1, 10, 50, and 100 mPa s under the same conditions, as the approach angle increases. As the approach angle increases, the smaller the crack width, the weaker stratification is less prone to shear failure; the greater the viscosity of the fracturing fluid, the greater the resistance of the crack flow, the greater the fluid pressure in the joint, the greater the width of the hydraulic crack, the hydraulic power. The more severe the passivation phenomenon of the crack in the weak bedding, the greater the shear stress of the weak bedding, the more likely the shear failure occurs [23–25]. Therefore, from the angle analysis of the shearing slip of the bedding plane to increase the complexity of the crack, increasing the viscosity of the fracturing fluid strongly enhances the complexity of the hydraulic fracture.

5.3. Influence of injection flow rate on interface shear failure

The injection flow has a certain influence on the hydraulic fracture propagation pattern. The other parameters are set unchanged, and the injection flow rate is changed. The calculation results are shown in Figs. 18 and 19.

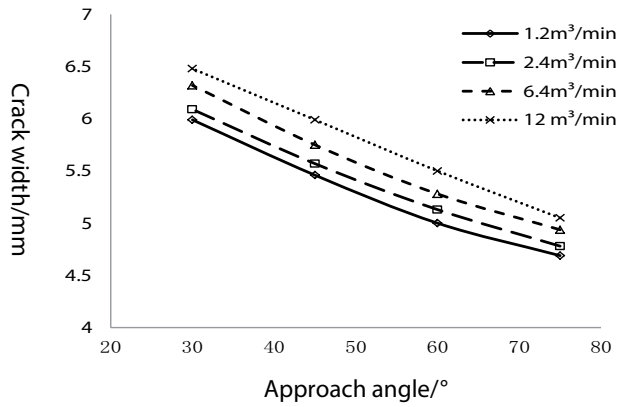

Fig. 18. Hydraulic crack width under different injection flows.

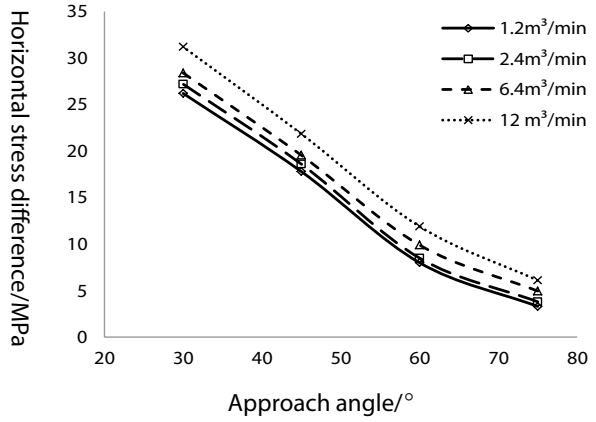

Fig. 19. Weak bedding shear failure conditions under different injection flows.

It can be seen from Figs. 18 and 19 that under the same injection flow rate, as the approach angle increases, the crack width is smaller, and the weak stratification is less prone to shear failure; as the injection flow rate increases, the hydraulic crack width increases [26–28]. The greater the horizontal principal stress difference required for shear failure, weak stratification is more susceptible to shear failure.

6. Conclusion

- Based on the fracture mechanics and seepage theory, the mechanical model of shear failure caused by hydraulic fracture activation is established, and the numerical simulation analysis is used to form the simulation method of hydraulic fracture expansion under the action of layered surface, obtained by the action law of hydraulic crack and weak bedding coupling.
- As the hydraulic fracture gradually approaches the weak bedding, the shear strength of the weak bedding surface gradually decreases. When the hydraulic fracture and the weak bedding meet, the hydraulic crack tip is passivated at the weak bedding, causing the increase of the weak bedding shear stress, and the weak bedding on the front side of the hydraulic crack expansion direction gradually reaches the shear strength and shear damage occurs.
- The larger the approach angle of hydraulic fracture and weak bedding, the greater the elastic modulus of the reservoir and the smaller the difference in geostress; the smaller the degree of passivation of hydraulic cracks and weak bedding, the less likely it is to induce weak bedding shear failure. The greater the viscosity of the fracturing fluid and the greater the displacement of the fracturing fluid, the easier it is to induce shear failure of the weak bedding plane, and the more complicated the fracture is formed, Therefore, for dense reservoirs dominated by bedding planes, it is suitable to use high-displacement and high-viscosity fracturing to activate weak bedding to form complex cracks.

Acknowledgement

National Key Basic Research and Development Program (973) Project (2015CB250900); National Natural Science Foundation of China (51374074).

References

[1] Z. Rusheng, W. Qiang, Z. Zuguo, Numerical simulation of three-dimensional extended ABAQUS of hydraulic fracturing fractures, Oil Drill. Process, 34 (2012) 69–72.
[2] Z. Guangming, L. He, Z. Jin, Three-dimensional finite element numerical simulation of hydraulic fracturing in horizontal wells, Eng. Mech., 28 (2011) 101–106.
[3] Z. Guanyu, W. Ruihe, Z. Weidong, Analysis of natural fracture failure characteristics under artificial crack approximation, Rock Soil Mech., 37 (2016) 247–255.
[4] H.D. Murphyhd, M.C. Fehler, Hydraulic Fracturing of Jointed Formations, Society of Petroleum Engineers International Meeting on Petroleum Engineering, Beijing, 1986.
[5] N.R. Warpinski, L.W. Teufel, Influence of geologic discontinuities on hydraulic fracture propagation, J. Petrol. Technol., 39 (1987) 209–220.
[6] A.A. Daneshy, Off-balance growth: a new concept in hydraulic fracturing, J. Pet. Technol, 55 (2003) 78–85.
[7] A.A. Daneshy, Analysis of Off-Balance Fracture Extension and Fall-Off Pressures, SPE 86471, 2004.
[8] Z. Jian, C. Mian, J. Yan, Study on shear failure mechanism of natural cracks in fracturing, J. Rock Mech. Eng., 27 (2008) 2637–2641.
[9] W. Rui, Study on Shear-Slip Mechanism of Hydraulic Fracture in Shale Formation, Southwest Petroleum University, Chengdu, 2015.
[10] C.D. Anderson, Effects of friction on hydraulic fracture growth near unbounded interfaces in rocks, Soc. Pet. Eng. J., 21 (1981) 21–29.
[11] C.E. Renshaw, D.D. Pollard, An experimentally verified for propagation across unbounded frictional interfaces in brittle, linear elastic materials, Int. J. Rock Mech. Min. Sci. Geom. Abstr., 32 (1995) 237–249.
[12] P. Chunyao, Study on interference mechanism of hydraulic fracturing cracks and weak surface of rock mass in layered shale, Oil Drill. Technol., 42 (2014) 32–36.
[13] C. Wan, J. Yan, C. Mian, Criteria for the penetration of hydraulic cracks into natural cracks in three-dimensional space, Petrol. Explor. Develop., 41 (2014) 336–340.
[14] L. Yongming, X. Wenjun, Z. Jinzhou, Judging criteria for hydraulic fractures in shale reservoirs passing through natural fractures, Nat. Gas Ind. B, 35 (2015) 49–54.
[15] X. De, Q. Qin, L. Changan, Numerical Calculation Method and Engineering Application in Fracture Mechanics,Science Press, Beijing, 2009.

[16] K. Atkinson, Y. Xiangchu, X. Jigang, Rock Fracture Mechanics, Seismological Press, Beijing, 1992.
[17] W. Wei, Numerical Simulation of Vertical Fracture Morphology and Seam Height Control of Hydraulic Fracturing, University of Science and Technology of China, Hefei, 2013.
[18] Y. Qiang, C. Xin, Z. Weiwei, Anisotropic yield criterion of jointed rock mass based on second-order damage tensor, J. Rock Mech. Eng., 24 (2005) 1275–1282.
[19] P. Khare, A. Singh, S. Verma, A. Bhati, A.K. Sonker, K.M. Tripathi, S.K. Sonkar, Sunlight-induced selective photocatalytic degradation of methylene blue in bacterial culture by pollutant soot derived nontoxic graphene nanosheets, ACS Sustainable Chem. Eng., 6 (2018) 579–589.
[20] L.-Z. Guo, C. Han, D.M. Wei, Empirical research on the relationship between natural gas consumption and economic growth in the Northeast Asia, Energy Environ., 29 (2018) 216–231.
[21] Y. Shen, N. Zhao, M. Xia, X. Du, A deep q-learning network for ship stowage planning problem, Polish Marit. Res., 24 (2017) 102–109.
[22] I.P.V.D. Pont, A.T. Caselli, S.M. Moreiras, C. Lauro, Recent coastal geomorphological evolution in the Negro River's mouth (41°S), Argentinean Patagonia, J. Coast. Res., 33 (2017) 1367–1375.
[23] I. syafiqah, H.W. Yussof, The use of factorial design for analysis of mercury removal efficiency using palm oil fuel ash, Water Conserv. Manage., 2 (2018) 10–12.
[24] Z.A.Z. Abidin, A.J.K. Chowdhury, Heavy metals and antibiotic resistance bacteria in marine sediment of pahang coastal water, J. CleanWAS, 2 (2018) 20–22.
[25] H. Amin, B.A. Arain, T.M. Jahangir, M.S. Abbasi, F. Amin, Accumulation and distribution of lead (Pb) in plant tissues of guar (*Cyamopsis tetragonoloba L.*) and sesame (*Sesamum indicum L.*): profitable phytoremediation with biofuel crops, Geol. Ecol. Landscapes, 2 (2018) 51–60.
[26] P.K. Rai, A. Rai, S. Singh, Change in soil microbial biomass along a rural-urban gradient in Varanasi (U.P., India), Geol. Ecol. Landscapes, 2 (2018) 15–21.
[27] M. Bahmani, A. Noorzad, J. Hamedi, F. Sali, The role of bacillus pasteurii on the change of parameters of sands according to temperature compression and wind erosion resistance, J. CleanWAS, 1 (2017) 1–5.
[28] B.S. Ismail, S.H. Haron, Heavy metal and insecticide distribution and accumulation at the Bertam agricultural watershed in Cameron Highlands, Pahang, Malaysia, Water Conserv. Manage., 1 (2017) 4–6.